INTERNATIONAL JOURNAL OF CLIMATOLOGY
Int. J. Climatol. **35**: 583–595 (2015)
Published online 7 April 2014 in Wiley Online Library
(wileyonlinelibrary.com) DOI: 10.1002/joc.4005

RMetS
Royal Meteorological Society

Comparative analysis of the ability of a set of CMIP3 and CMIP5 global climate models to represent precipitation in South America

Carla Gulizia[a,b,c]* and Inés Camilloni[a,b,c]

[a] *Departamento de Ciencias de la Atmósfera y los Océanos, Facultad de Ciencias Exactas y Naturales, Universidad de Buenos Aires, Buenos Aires, Argentina*

[b] *Centro de Investigaciones del Mar y la Atmósfera (CIMA), Universidad de Buenos Aires, Consejo Nacional de Investigaciones Científicas y Técnicas, Buenos Aires, Argentina*

[c] *UMI IFAECI/CNRS, Buenos Aires, Argentina*

ABSTRACT: The purpose of this study is to evaluate the ability of two sets of global climate models (GCMs) derived from the Coupled Model Intercomparison Projects Phase 3 (CMIP3) and Phase 5 (CMIP5) to represent the summer, winter, and annual precipitation mean patterns in South America south of the equator and in three particular sub-regions, between years 1960 and 1999. Different metrics (relative bias, spatial correlation, RMSE, and relative errors) were calculated and compared between both projects to determine if there has been improvement from CMIP3 to CMIP5 models in the representation of regional rainfall. Results from this analysis indicate that for the analysed seasons, precipitation simulated by both CMIP3 and CMIP5 models' ensembles exhibited some differences. In DJF, the relative bias over Amazonia, central South America, eastern Argentina, and Uruguay is reduced in CMIP5 compared with CMIP3. In JJA, the same occurs in some areas of Amazonia. Annual precipitation is also better represented by the CMIP5 than CMIP3 GCMs as they underestimate precipitation to a lesser extent, although in NE Brazil the overestimation values are much larger in CMIP5 than in CMIP3 analysis. In line with previous studies, the multi-model ensembles show the best representation of the observed patterns in most seasons and regions. Only in some cases, single GCMs [MIROC3.2(hires) – CMIP3– and MIROC4h – CMIP5] presented better results than the ensemble. The high horizontal resolution of these models suggests that this could be a relevant issue for a more adequate estimation of rainfall at least in the analysed regions.

KEY WORDS global climate models; evaluation; precipitation; South America; CMIP3; CMIP5

Received 23 November 2012; Revised 26 February 2014; Accepted 12 March 2014

1. Introduction

Quantitative predictive information on the effect of anthropogenic greenhouse gas emissions on the climate is required for both regional impact assessments and for developing tools to address adaptation to climate change. Climate projections are elaborated using global climate models (GCMs). Model confidence is usually based on the evaluation of their performance at reproducing observed features of current climate. Single models and multi-model ensembles are evaluated by using observationally based data sets and model intercomparison activities that contribute significantly to identify model's relative biases. GCMs' ability to simulate past climate and its variability is limited by some aspects of the modelling procedure such as the choice of grid resolution and the parameterizations of processes unresolved at the grid scale. Furthermore, limitations in the scientific understanding of some physical processes also affect model performance. The GCMs used for the preparation of the IPCC Fourth Assessment Report (AR4) (IPCC, 2007), available from the World Climate Research Programme–Coupled Model Intercomparison Project Phase 3 data set (WCRP-CMIP3; Meehl *et al.*, 2007), can simulate the large-scale mean climate conditions of the planet and its evolution to a great extent. Nevertheless, their ability to simulate climate features at a regional scale is limited (Boulanger *et al.*, 2007; Silvestri and Vera, 2008; Sakaguchi *et al.*, 2012; Gulizia *et al.*, 2013). A new generation of simulations, known as CMIP Phase 5 (CMIP5; Stouffer *et al.*, 2011; Taylor *et al.*, 2012), has recently become available for analysis through the Program for Climate Model Diagnosis and Intercomparison (PCMDI, http://cmip-pcmdi.llnl.gov/cmip5/). Relative to CMIP3, CMIP5 constitutes an unprecedented set of experiments that include higher spatial resolution models and improved model physics. However, it is necessary to evaluate the

* Correspondence to: C. Gulizia, Centro de Investigaciones del Mar y la Atmósfera (CIMA), Universidad de Buenos Aires, Consejo Nacional de Investigaciones Científicas y Técnicas, Buenos Aires, Argentina. E-mail: gulizia@cima.fcen.uba.ar

ability of CMIP5 to simulate present climate at both global and regional level, and to assess the improvement of CMIP5 models, relative to those of CMIP3. To our knowledge, only a few studies have examined the ability of CMIP5 experiments to represent the 20th century climate at regional scale over South America (Wilcox *et al.*, 2012; Yin *et al.*, 2012; Joetzjer *et al.*, 2013; Jones and Carvalho, 2013). Those studies were mainly focused on a particular region as the Amazonia (Yin *et al.*, 2012; Joetzjer *et al.*, 2013) or on climatic features as the South American monsoon system (SAMS) (Jones and Carvalho, 2013) or the austral jet (Wilcox *et al.*, 2012). Consequently, there is still a lack of evaluation of the CMIP5 models both at continental scale and/or in a relevant region as southeastern South America (SESA), which is the most important area of the continent in terms of socio-economic activities with over 100 million inhabitants. SESA also hosts La Plata Basin with almost a hundred dams and more than 30 large hydropower plants, which contribute with 55.5% of the total energy demand in the region (Popescu *et al.*, 2012). During the last decades, SESA has been subject to climate trends that could be related to the increase in atmospheric concentration of anthropogenic greenhouse gases. Examples of changes are increased precipitation (Giorgi, 2002; Berbery *et al.*, 2006; Haylock *et al.*, 2006; Re and Barros, 2009; Marengo *et al.*, 2010), river flow variability (Barros, 2006; Doyle and Barros, 2011), and extreme temperatures (Rusticucci and Barrucand, 2004; Marengo *et al.*, 2010).

The main objective of this study is to assess the ability of two sets of CMIP3 and CMIP5 GCMs to represent the spatial patterns of summer, winter, and annual mean precipitation in South America, south of the equator. Moreover, three sub-regions are evaluated in more detail: central South America (CSA), southeast Brazil (SEBR), and the southern sector of SESA (SSESA). CSA coincides with the continental core of the monsoon region during the warm season and SEBR matches the continental area of the South Atlantic Convergence Zone (SACZ). These particular regions were selected as they are associated with key climatic features of the continent (SAMS and SACZ) or because of their strongly water-dependent socio-economic activities (SSESA). Various statistical analysis are presented to identify the more adequate GCMs to represent present climate in the study region, as well as to assess improvements in CMIP5 GCMs relative to those of CMIP3.

The article is structured in five sections. Data are described in Section 2 and the evaluation of South American rainfall at continental scale is presented in Section 3. Section 4 includes a regional analysis focused on three particular sub-regions and Section 5 summarizes results and conclusions.

2. Data

This study is based on a comparison between 19 GCMs from the WCRP-CMIP3 multi-model data set and an equal number of models available from CMIP5, during the period 1960–1999. We analysed the representation of the mean spatial patterns of the austral summer (December, January, February – DJF), winter (June, July, August – JJA), and annual accumulated precipitation in South America, south of the equator by each set of models. Observed precipitation data used for the evaluation were obtained from the $0.5^\circ \times 0.5^\circ$ gridded monthly data set TS3.10 produced by the Climate Research Unit (CRU) using the daily data available for the period 1901–2009 (Harris *et al.*, 2013). Table 1 shows a short description of the analysed models from CMIP3, indicating their resolution and the institution where they were generated. We used 20th-century simulations known as 20C3M, which start with pre-industrial conditions during the end of the 19th century and end in the year 2000, including both natural and anthropogenic forcing. CMIP5 GCMs considered in this study are listed in Table 2. Eight of these new-generation models belong to the same institutions as those analysed from the CMIP3 data set (Tables 1 and 2). The CMIP5 versions include changes in the spatial resolutions and physical process descriptions as well as new model components. Although a detailed analysis of the major improvements in each single model is out of the scope of this study, it is important to highlight that most of them exhibit increases in the horizontal resolution and/or in the number of vertical levels and also shifts of the top grid to higher levels (Flato *et al.*, 2013). In addition, some of them also include new physical parameterizations (cumulus convection scheme or a high accuracy radiation scheme) (Dufresne *et al.*, 2013), new land models (Delworth *et al.*, 2006; Watanabe *et al.*, 2011), and aerosol effects on clouds (Bellouin *et al.*, 2007; Dufresne *et al.*, 2013).

The analysed simulations include natural and anthropogenic forcing and are part of the *historical* experiment that starts in the year 1850 and ends in 2005. In this study, only one run of each model – identified as *run1* and *r1i1p1* for CMIP3 and CMIP5, respectively – was considered. Multi-model ensemble means were computed for both sets of 19 GCMs as well as for the subset of 8 models that belong to the same institutions in both generations in order to evaluate possible improvements in the representation of regional rainfall.

In addition to the evaluation analysis over South America, three sub-regions were considered (Figure 1). The CSA sub-region is encompassed between 50°W–60°W and 10°S–20°S; the SEBR sub-region is limited by 40°W–50°W and 15°S–25°S; and the SSESA sub-region corresponds to the southern sector of SESA, between 50°W–60°W and 22.5°S–35°S. The three sub-region boundaries concur with those defined by different authors (Gan *et al.*, 2006; Seth *et al.*, 2010). We transformed the observed and GCM-generated data to a common grid of $2.5^\circ \times 2.5^\circ$ using the Kriging interpolation method, and then compared the mean spatial patterns of seasonal and annual precipitation.

Table 1. CMIP3 models analysed in this study.

Model ID, *Vintage*	Sponsor(s), country	Lon × lat levels, atmospheric resolution
CGCM3.1(T47), 2005	Canadian Centre for Climate Modelling and Analysis, Canada	96 × 48, L32
CGCM3.1(T63), 2005 (*)		128 × 64, L31
CNRM-CM3, 2004	Metéo-France/Centre National de Recherches Météorologiques, France	128 × 64, L45
CSIRO-MK3.0, 2001	Commonwealth Scientific and Industrial Research Organisation (CSIRO) Atmospheric Research, Australia	128 × 64, L18
ECHAM5/MPI-OM, 2005	Max Planck Institute for Meteorology, Germany	128 × 64, L31
GFDL-CM2.0, 2005 (*)	U.S. Department of Commerce/National Oceanic and Atmospheric Administration (NOAA)/Geophysical Fluid Dynamics Laboratory (GFDL), USA	144 × 90, L24
GFDL-CM2.1, 2005		144 × 90, L24
GISS-AOM, 2004	National Aeronautics and Space Administration (NASA)/Goddard Institute for Space Studies (GISS), USA	90 × 60, L12
GISS-EH, 2004		72 × 46, L20
GISS-ER, 2004 (*)		72 × 46, L20
INGV-SXG, 2005	Instituto Nazionale di Geofisica e Vulcanologia, Italy	320 × 160, L19
INM-CM3.0, 2004 (*)	Institute for Numerical Mathematics, Russia	72 × 46, L21
IPSL-CM4, 2005 (*)	Institut Pierre Simon Laplace, France	96 × 72, L19
MIROC3.2(hires), 2004 (*)	Center for Climate System Research (University of Tokyo), National Institute for Enviromental Studies, and Frontier Research Center for Global Change (JAMSTEC), Japan	320 × 160, L56
MIROC3.2(medres), 2004		128 × 64, L20
MRI-CGCM2.3.2, 2003 (*)	Meteorological Research Institute, Japan	128 × 64, L30
NCAR-PCM1, 1998	National Center for Atmospheric Research, USA	128 × 64, L26
UKMO-HadCM3, 1997	Hadley Centre for Climate Prediction and Research/Met Office, UK	96 × 72, L19
UKMO-HadGEM1, 2004 (*)		192 × 144, L38

Also listed are the respective sponsoring institutions and the number of points in the latitude by number of points in the longitude. Vertical resolution (L) is the number of vertical levels. GCMs indicated with (*) correspond to those which were considered for the eight GCMs' subset.

3. Rainfall evaluation at continental scale

South American precipitation has a well-defined annual cycle determined by the yearly variations of the atmospheric circulation over the continent and the adjacent oceans. Figure 2 shows the summer, winter, and annual mean precipitation in South America, south of 0°. The spatial distribution of summer rainfall north of 20°S is above 400 mm, except over NE Brazil (Figure 2(a)). Moreover, east of 60°W comparable rainfall values extend to 30°S. In Uruguay and the north-central part of Argentina, east of the Andes Mountains, the accumulated rainfall is between 200 and 400 mm, whereas south of 40°S in the Andes precipitation is minimal during this season, with values below 100 mm. During winter, the highest rainfall values are observed in SSESA and north of 5°S, exceeding 200 mm in some regions (Figure 2(b)). Along the southern Andes, the maximum precipitation occurs also during this season, mainly produced by frontal systems. The annual rainfall pattern shows a maximum over NW South America, exceeding 2000 mm and a secondary maximum above 1000 mm over SSESA (Figure 2(c)). In western Argentina and part of the Andes, annual precipitation is below 200 mm, except west of 70°W between 40°S and 50°S, where values are above 1000 mm. This maximum precipitation is due to the enhanced uplift over the Andes western slopes (Lenters and Cook, 1995), which produces dry conditions leeward.

In order to evaluate the accuracy of the CMIP3 and CMIP5 GCMs in describing the seasonal variability and the main climatic features of rainfall over South America presented in Figure 2(a)–(c), the relative biases between the ensemble means of the selected 19 GCMs from each intercomparison project and the observations were computed. These biases were calculated considering the percentages of annual and seasonal observed rainfall that are represented by each ensemble mean and for each grid point using the following expression:

$$\text{Relative bias} = \frac{\text{Precipitation}_{\text{GCMs}}}{\text{Precipitation}_{\text{CRU}}} \times 100 - 100 \qquad (1)$$

Figure 2 shows the spatial patterns of CMIP3 (Figure 2(d)–(f)) and CMIP5 (Figure 2(g)–(i)) GCMs' relative biases for summer, winter, and annual rainfall. For the analysed seasons, precipitation simulated by both models' ensembles exhibited some differences. In DJF, the relative bias over Amazonia, central South America, eastern Argentina, and Uruguay is reduced in CMIP5 compared with CMIP3. In JJA, the same occurs in some areas of Amazonia. The magnitude and spatial distribution of overestimation (positive relative biases) and underestimation (negative relative biases) patterns relative to observations were comparable in both models. The largest relative biases include excessive precipitation over northeastern Brazil, and the southern sector of the continent, and precipitation deficit over the Amazonia and central and SESA. On the other hand, the underestimation over the Amazonia and the SEBR sub-region could not be completely associated with a poor representation of convection by the GCMs' parameterizations as the lowest relative biases were found during summer when convection is more intense. In these regions, the largest

Table 2. CMIP5 models analysed in this study.

Model ID, *Vintage*	Sponsor(s), country	Lon × lat levels, atmospheric resolution
BCC-CSM1.1, 2011	Beijing Climate Center, China Meteorological Administration, China	128 × 64, L26
CanESM2, 2010 (*)	Canadian Centre for Climate Modelling and Analysis, Canada	128 × 64, L35
GFDL-CM3, 2011 (#)	Geophysical Fluid Dynamics Laboratory (GFDL), USA	~200 km, L48
GFDL-ESM2G, 2011(#)		2° × 2.5°, L24
GFDL-ESM2M, 2011 (*)		144 × 90, L24
GISS-E2-H, 2004	NASA Goddard Institute for Space Studies, USA	144 × 90, L40
GISS-E2-R, 2011 (*)		144 × 90, L40
HadCM3, 1998	UK Met Office Hadley Centre, UK	96 × 72, L19
HadGEM2-CC, 2010		192 × 144, L60
HadGEM2-ES, 2009 (*)		192 × 144, L38
INMCM4, 2009 (*)	Russian Institute for Numerical Mathematics, Russia	180 × 120, L21
IPSL-CM5A-LR, 2010 (*)	Institut Pierre Simon Laplace, France	96 × 95, L39
IPSL-CM5A-MR, 2009		144 × 143, L39
MIROC4h, 2009	University of Tokyo, National Institute for Environmental Studies, and Japan Agency for Marine-Earth Science and Technology, Japan	128 × 64, L80
MIROC5, 2010		128 × 64, L80
MIROC-ESM, 2010 (*)		640 × 320, L56
MIROC-ESM-CHEM, 2010		256 × 128, L40
MRI-CGCM3, 2011 (*)	Meteorological Research Institute, Japan	320 × 160, L48
NorESM1-M, 2011	Norwegian Climate Centre, Norway	144 × 96, L26

Also listed are the respective sponsoring institutions and the number of points in the latitude by number of points in the longitude. Vertical resolution (L) is the number of vertical levels. GCMs indicated with (*) correspond to those which were considered for the eight GCMs' subset. (#) GCMs' horizontal resolution indicated in different units as available in literature.

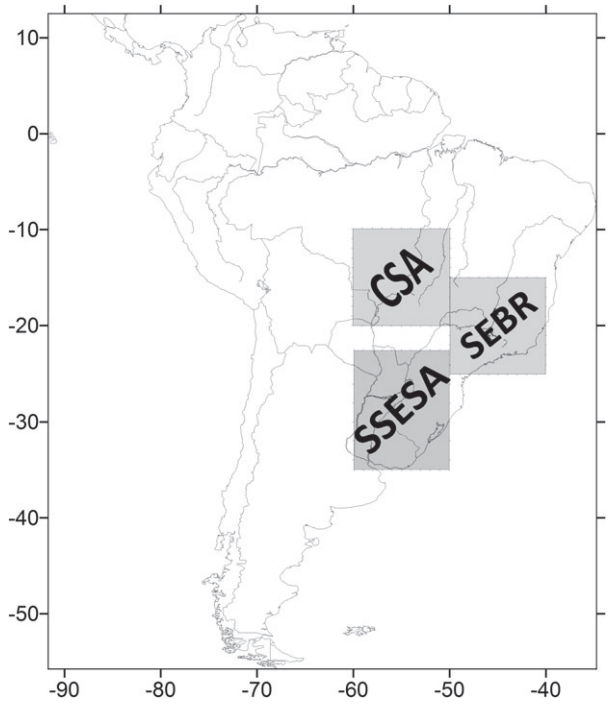

Figure 1. Study area and sub-regions (central South America – CSA, southeastern Brazil – SEBR, and southern sector of southeastern South America – SSESA) considered.

relative biases occurred during the dry season when observed rainfall is very low. The large overestimation in precipitation over the Andes was also identified by different authors considering both global and regional models, probably due to their inadequacies in the representation of complex topography and the associated circulation and moisture transport (Alves and Marengo, 2010; Insel *et al.*, 2010). The same reasons could explain the overestimation of precipitation in the area to the south of 40°S, where the Andes block the transport of humid air by the westerlies producing dry conditions in the Argentinean region, east of the Andes (Prohaska, 1976). Nevertheless, the results described previously are to some extent conditioned by the low quality of the observational data set in the Andean mountainous area and the southern tip of the continent, due to the limited number of gauging stations in these areas.

Our comparison between the two GCMs' ensembles relative biases shows that CMIP5 exhibits an improved simulation of summer precipitation, especially over the Amazon region and SSESA. CMIP5 also showed a better winter rainfall estimation over parts of the Amazonia relative to CMIP3. However, both ensembles produced similar relative biases in their representations of precipitation in northeastern Brazil, the regions over and near the Andes, and the southern tip of the continent south of 40°S, in particular for the winter spatial pattern, showing overestimations larger than 300%.

The linear spatial correlation coefficients (R) between the observed and GCMs' ensemble rainfall for the region delimited by 80°W–35°W and 2.5°S–52.5°S are also indicated in Figure 2. In all cases, these coefficients are statistically significant at the 95% level. The CMIP5 representation of winter precipitation in parts of the Amazonia showed higher spatial correlation

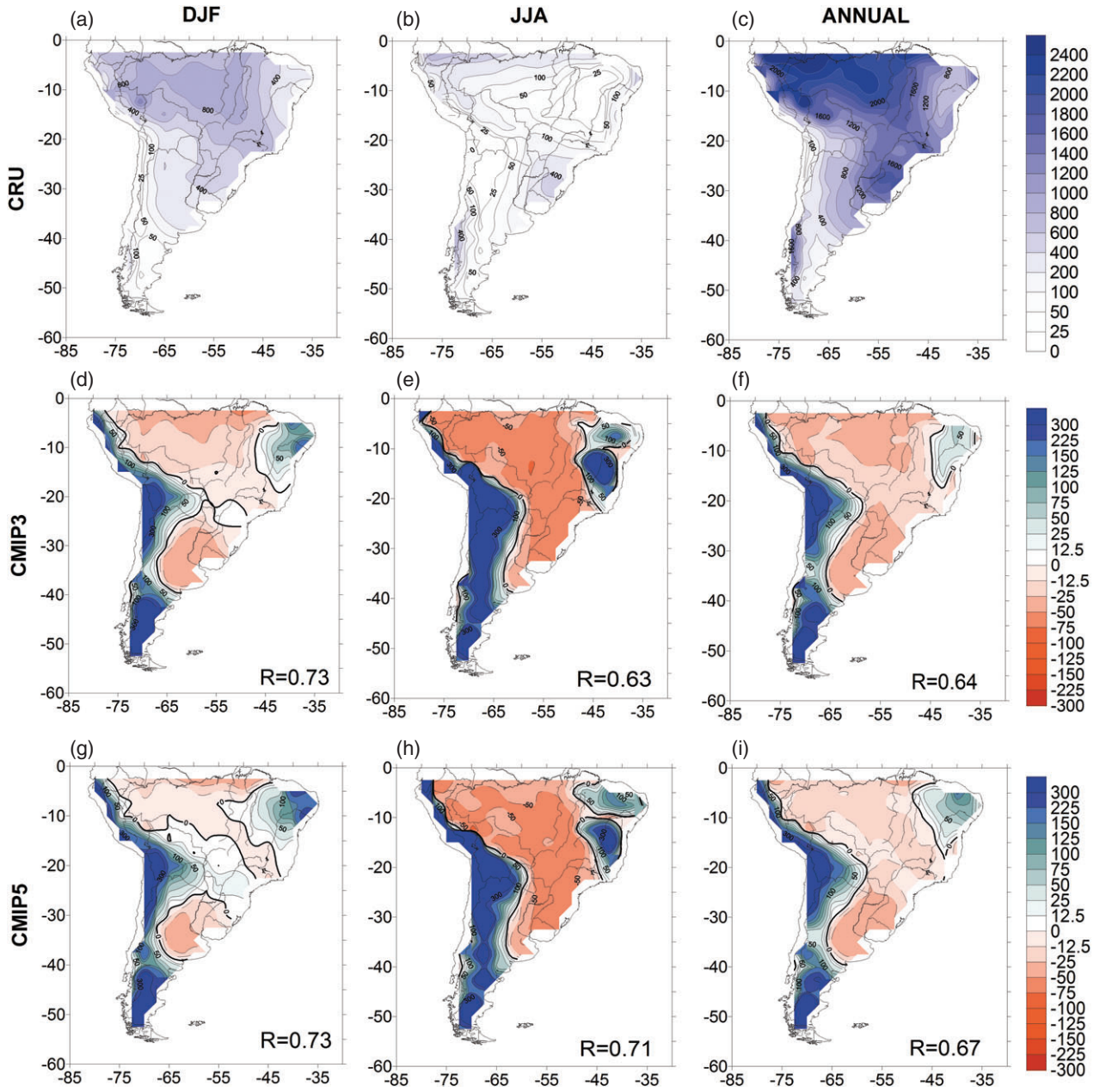

Figure 2. Accumulated mean precipitation derived from the CRU data set for (a) summer, (b) winter (mm season^{-1}), and (c) annual mean (mm year^{-1}). Biases (%) of summer, winter, and annual precipitation for the CMIP3 [(d), (e), and (f), respectively] and CMIP5 [(g), (h), and (i), respectively] 19 GCMs' ensemble. The linear spatial correlation coefficient (R) between the observations (CRU data set) and each of the GCMs' ensembles is also included.

than in the CMIP3 case. The individual performance of each GCM considered in both ensembles presented in Figure 3 was analysed by computing the linear spatial correlation coefficients between the observed and simulated seasonal and annual rainfall patterns. Four of the CMIP3 models (ECHAM5/MPI-OM, UKMO-HadCM3, UKMO-HadGEM1, and MRI-CGCM2.3.2) and the ensemble mean of 19 GCMs showed statistically significant linear correlation coefficients at the 95% level ($R > 0.60$) for both seasons and the annual mean precipitation (Figure 3(a)). Furthermore, only the MRI-CGCM2.3.2 model shows higher correlation coefficients than the ensemble in all cases, and the GISS-AOM model has the lowest linear correlation coefficients indicating the largest deficiencies in representing the seasonal and annual mean precipitation fields.

In the case of CMIP5, three individual models (HadCM3, HadGEM2-CC, and HadGEM2-ES) and the ensemble means of both the 8 and 19 GCMs are able to represent reasonably well ($R > 0.60$) the summer, winter, and annual precipitation in South America, south of 0° (Figure 3(b)). In this case, only the HadGEM2-ES model shows higher correlation coefficients than the ensemble means in all cases.

We also compared the ability of CMIP3 and CMIP5 individual GCMs and ensemble mean to simulate seasonal

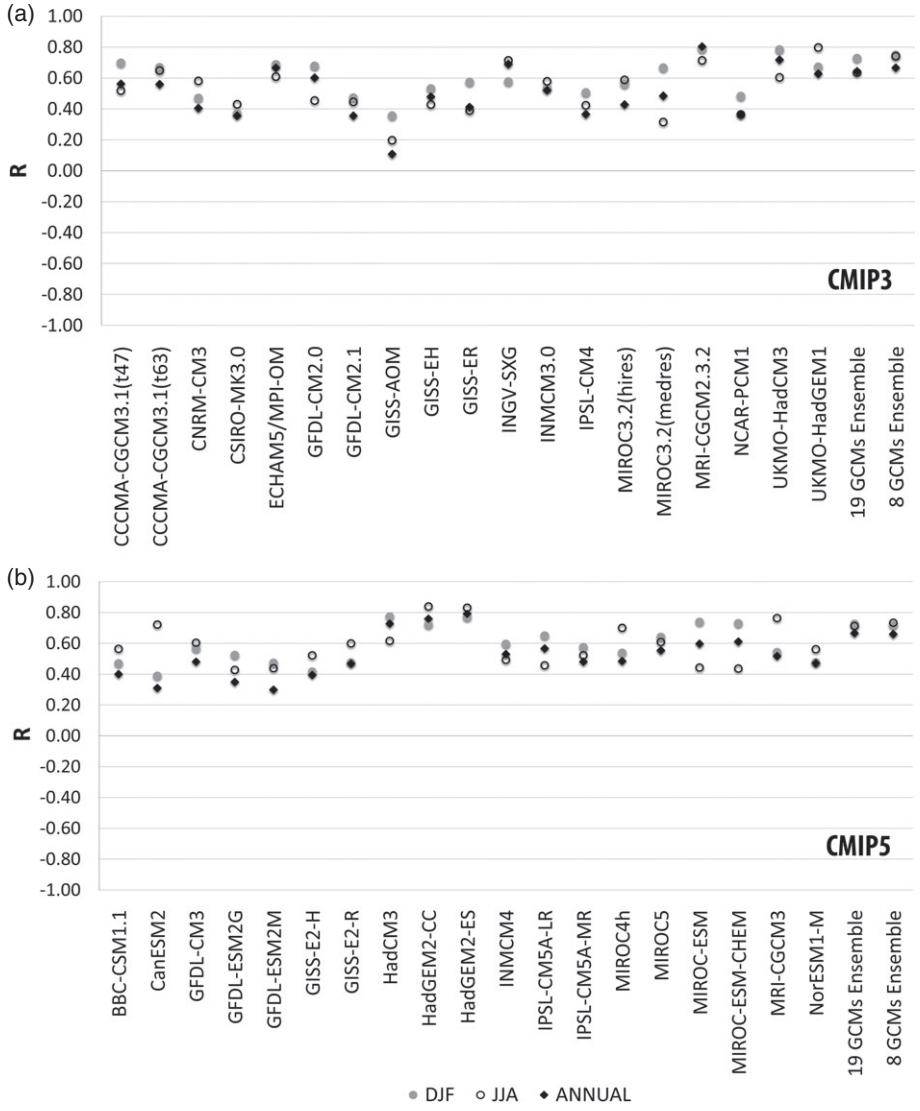

Figure 3. Linear spatial correlation coefficients (R) between the observed and simulated rainfall from individual GCMs for summer, winter, and annual mean values for (a) CMIP3 and (b) CMIP5 models for South America, south of the equator. R coefficients corresponding to the 19 and 8 GCMs' ensemble means are also included.

and annual precipitation in South America by computing the root-mean-square error normalized by the range of observed data (nRMSE) in each case. This statistical measure has been used by different authors (e.g. Gleckler *et al.*, 2008; Pincus *et al.*, 2008; Su *et al.*, 2013) to evaluate simulated precipitation against observations both at the global and regional scales. As there are some discrepancies regarding the best metrics to evaluate climate simulations (Willmott and Matsuura, 2005; Schaller *et al.*, 2011), we used a set of different statistical measures (relative bias, spatial correlation, nRMSE, and relative errors). Figure 4 shows the nRMSE and the median errors. We did not use mean errors to minimize the influence of models with large errors (outliers). The median nRMSEs of the 19 CMIP5 models are higher for summer, winter, and the annual mean than for the CMIP3 models. However, the errors of the ensemble mean are lower for CMIP5 models for the winter and annual cases. The same results were observed when considering the subset of eight GCMs.

A relative error (E'_{mt}) for a given model m and time period t (season/year) is computed according to Gleckler *et al.* (2008) as

$$E'_{mt} = \frac{E_{mt} - \overline{E}_t}{\overline{E}_t} \tag{2}$$

where E_{mt} is the RMSE of the model m at the time period t and $\overline{E}_t$ is the median of the RMSE of the N GCMs considered ($N = 8$ or 19 for each intercomparison project) and represents the typical model error at the same time t. E'_{mt} is a metric which indicates how well a given model (relative to CRU precipitation) compares with the typical model error. Negative (positive) values indicate that the model's nRMSE is lower (higher) than the typical error. Figure 5 shows the seasonal and annual models' relative errors for CMIP3 and CMIP5 GCMs. For both cases, the models' ensembles agree with observations better than the corresponding typical model. In addition, the MRI-CGCM2.3.2 model in the CMIP3 analysis (Figure 5(a)) exhibits a better

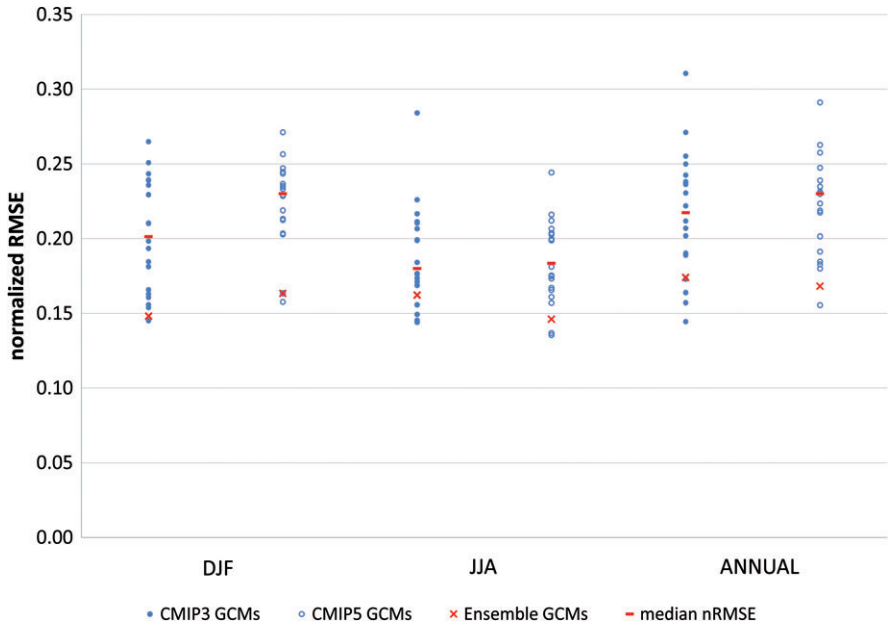

Figure 4. Normalized root-mean-square error (nRMSE) in simulating precipitation for individual CMIP3 (filled circles) and CMIP5 (empty circles) GCMs and for the 19 GCMs' ensemble means (crosses). Normalization was done by the range of observed data. The median errors (dashes) corresponding to each intercomparison projects are also included.

performance than the multi-model ensemble, while there is no individual model in the set of CMIP5 GCMs analysed showing better agreement to observations than the ensemble (Figure 5(b)).

4. Evaluation of rainfall in the CSA, SEBR, and SSESA sub-regions

This section presents the correlation analysis for the three relevant climatic sub-regions defined in Section 2 (CSA, SEBR, and SSESA). The results obtained for the CSA region must be taken with caution as the number of gauging stations available in this area is much more limited than in the SEBR and SSESA sub-regions, where observational data is more abundant and reliable.

In CSA (Figure 6(a)), 14 out of 19 CMIP3 GCMs, as well as the multi-model ensembles, represented adequately the summer precipitation spatial pattern, showing statistically significant linear correlation coefficients exceeding 0.60. Winter precipitation spatial pattern was also represented considerably well as ten GCMs, as well as the 19 models ensemble, showed significant linear correlation coefficient. Likewise, 13 GCMs were able to represent reasonably well the annual rainfall pattern ($R > 0.60$) in this region, with the highest linear coefficient corresponding to the ensembles of the 8 and 19 GCMs ($R = 0.96$).

During both summer and winter seasons, 14 CMIP3 GCMs showed R coefficient above 0.60 in SEBR (Figure 6(b)). Moreover, 12 models represented adequately the annual precipitation pattern, CCCMA-CGCM3.1, MIROC3.2(hires), and UKMO-HadCM3 showing the best performance ($R > 0.80$). The highest correlation coefficient was found for the ensemble of the set of eight GCMs ($R = 0.86$).

In SSESA, 17 CMIP3 GCMs showed R above 0.60 during summer, while there were 12 models during winter (Figure 6(c)). Furthermore, ten GCMs had linear correlation coefficients greater than 0.60 for the annual pattern, and ECHAM5/MPI-OM and MIROC3.2(hires) showed the best rainfall representation, with correlation coefficients of 0.77 and 0.88, respectively. In this case, the ensemble means were lower than those for the CSA and SEBR regions.

The same computations were conducted for the CMIP5 GCMs (Figure 6(d)–(f)). The multi-model ensembles showed an adequate representation ($R > 0.75$) of summer, winter, and annual precipitation in the three regions. For CSA, the two ensembles showed the highest correlation coefficients for both the summer and annual precipitation (Figure 6(d)). The same was observed for SEBR, with R values above 0.90 (Figure 6(e)). For SSESA, the ensemble showed the highest correlation values for winter (Figure 6(f)). Finally, in most seasons and regions, the amount of GCMs with statistically significant linear correlation coefficients in the spatial representation of precipitation was larger for the analysed CMIP5 models than for the CMIP3 ones. The only exception was the SEBR region during winter.

Area averages for the three analysed sub-regions of observed summer, winter, and annual precipitation, along with the median and the first and third quartile derived from the simulated precipitation by CMIP3 and CMIP5 models, are shown in Figure 7. Outlier models with extreme values (lower than the 10th percentile and greater than the 90th percentile) are also included in this Figure 7. We show the median of the simulated precipitation because it is a robust measure of the central tendency, and it is less affected by outliers than the mean. The interquartile

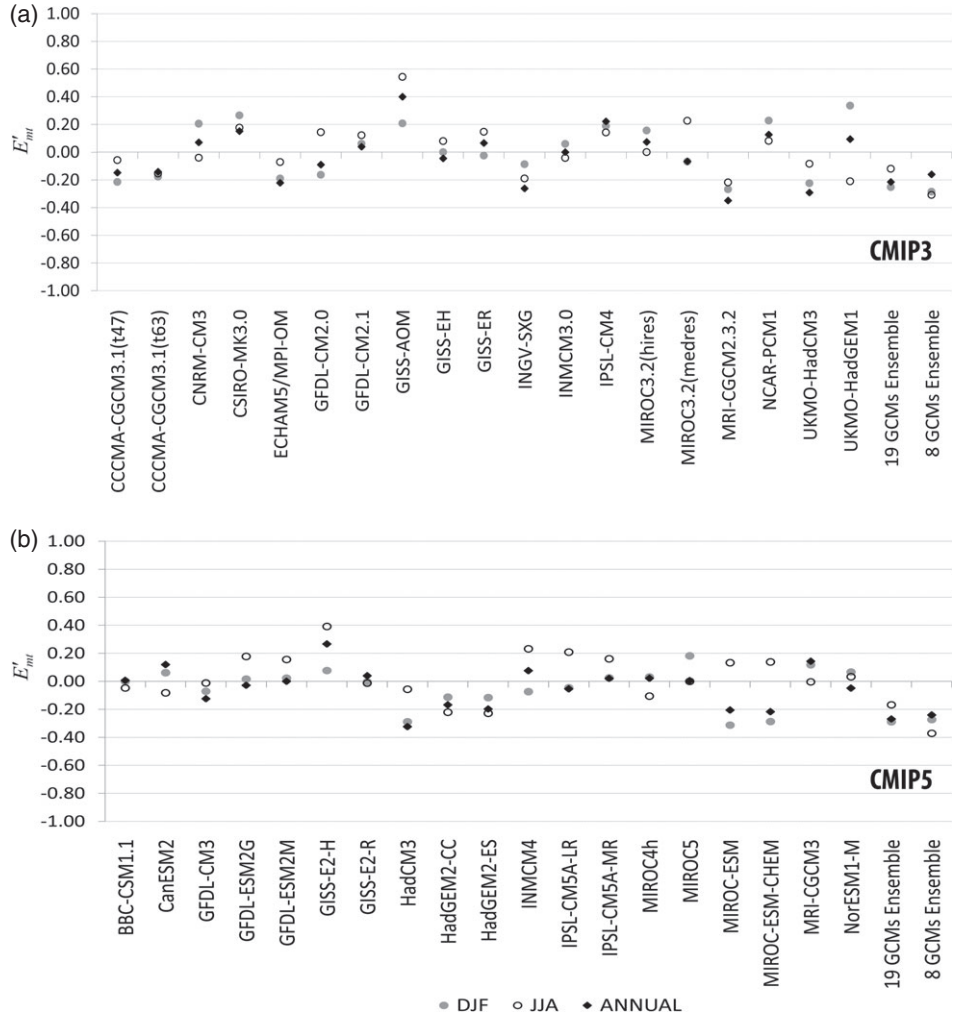

Figure 5. Seasonal and annual relative error (E'_{mt}) for individual (a) CMIP3 and (b) CMIP5 GCMs. The E'_{mt} corresponding to the 19 and 8 GCMs' ensemble means are also included.

interval (25–75%) is an adequate measure to evaluate the model's dispersion, as it excludes the values exceeding that range and it specifies the range of the central value of 50% thereof (Wilks, 1995).

Figure 7(a)–(c) shows that the distance between the CMIP3 GCMs' median and the mean observed precipitation differs in the three studied sub-regions and between seasons. In general, the median is always below observations, highlighting that all GCMs underestimate precipitation in the three sub-regions. This is consistent with the results of Figure 2. During summer, the median of the GCMs considerably approaches the observed precipitation (Figure 7(a)), especially in the SEBR and SSESA sub-regions, while the discrepancy between the median and the mean observations is greater in the CSA sub-region. However, even though the observed rainfall averages were within the interquartile range in all the sub-regions, these values were underestimated. For the winter (Figure 7(b)) and annual (Figure 7(c)) cases, observations were always above the third quartile and sometimes close to the extreme simulated values (outliers), indicating that most GCMs underestimated precipitation. Consequently, a model standing as an outlier does not necessarily imply a misrepresentation of the observed precipitation but instead shows significantly different regional simulated rainfall amounts than most of the analysed GCMs. Some examples are the CCCMA-CGCM3.1(t63) model for the annual simulated precipitation in SSESA, and the MRI-CGCM2.3.2 in the CSA region during winter.

Figure 7(d)–(f) shows a similar analysis for CMIP5 GCMs. The results indicated some improvements in the representation of both summer and annual precipitation in CMIP5. During summer (Figure 7(d)), the area mean of observations is within the interquartile range (as in the CMIP3 analysis), but the median of the simulations considerably approaches the average observations in the CSA and SEBR sub-regions and even more so in SSESA. During winter (Figure 7(e)), there were still difficulties in the estimation of precipitation in all regions, mostly in SSESA, with large underestimations consistent with the results of Figure 2. For the CMIP5 annual analysis, the median was closer (albeit lower) to the observations than for the CMIP3 GCMs. This result indicates that, even though CMIP5 models underestimate precipitation in the three regions, they do so to a lesser extent than in CMIP3.

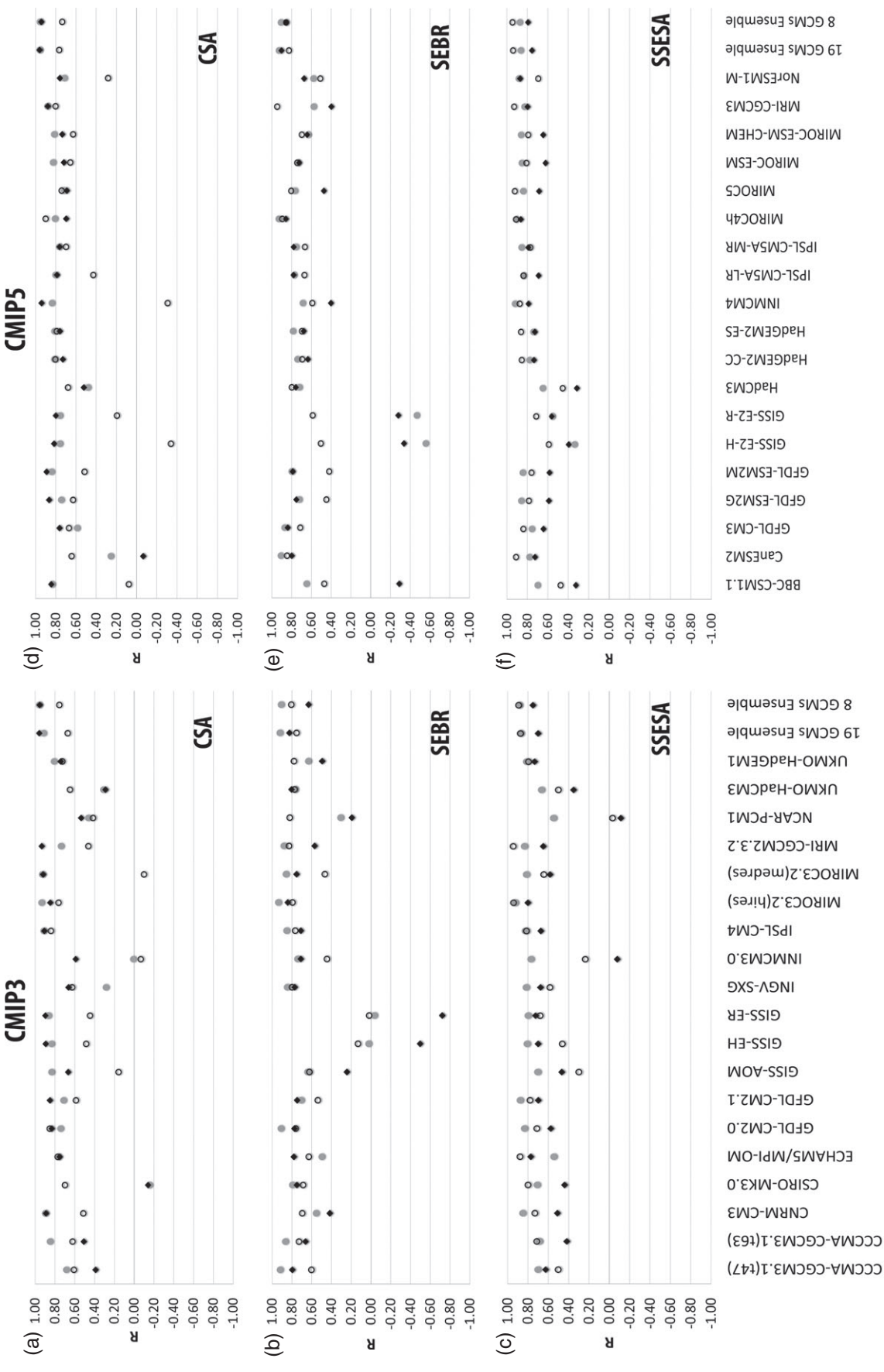

Figure 6. Linear spatial correlation coefficients (R) between the observed and simulated rainfall from individual GCMs for summer, winter, and annual mean values for the three sub-regions considered: (a) CSA, (b) SEBR, and (c) SSESA in CMIP3 analysis; (d) CSA, (e) SEBR, and (f) SSESA for the CMIP5 GCMs.

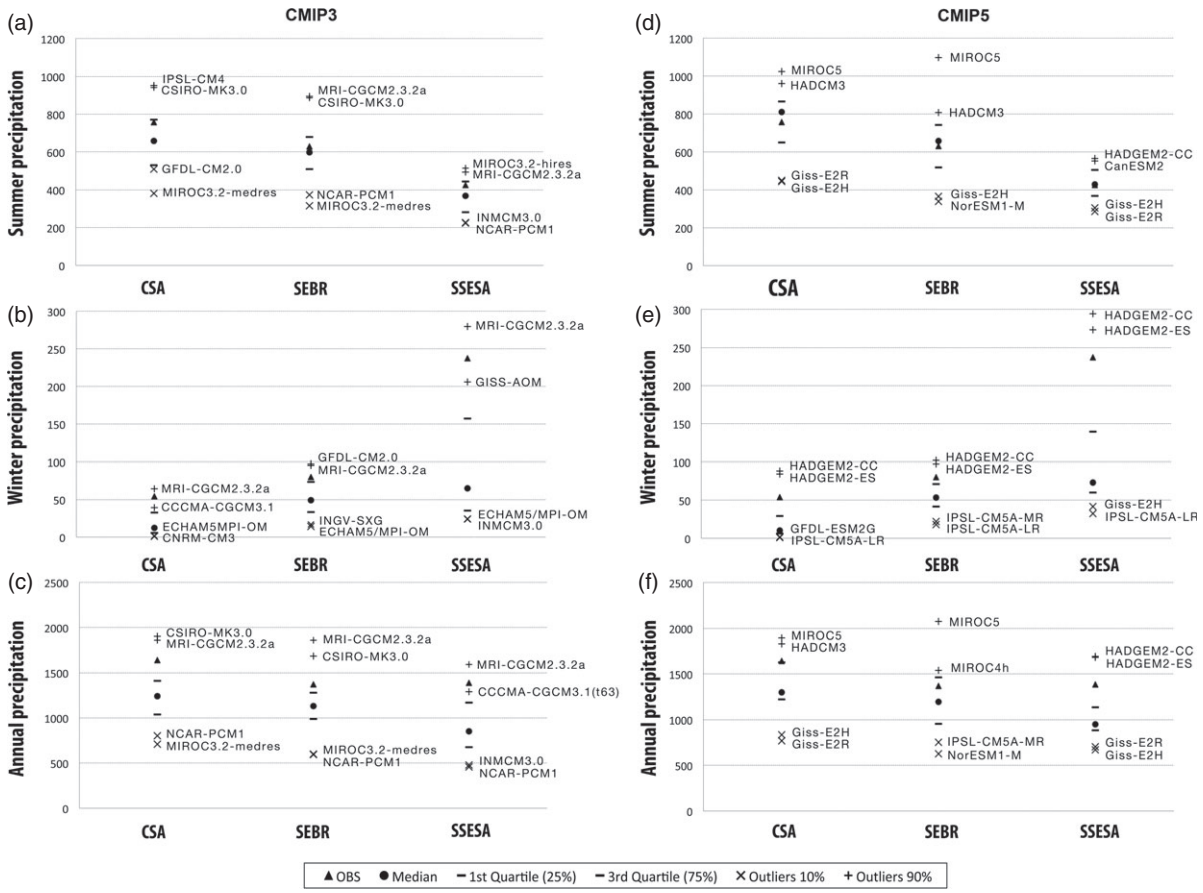

Figure 7. Areal averages (for the three analysed sub-regions) of observed summer, winter (mm season^{-1}) and annual (mm year^{-1}) precipitation, together with the median and the first and third quartile derived from the simulated precipitation derived from CMIP3 [(a), (b), and (c), respectively] and CMIP5 [(d), (e), and (f), respectively]. The outliers of the models which present extreme values lower than 10th percentile and greater than 90th percentile are also included.

In particular, the area average of annual observed precipitation in the SEBR region fell within the interquartile range, which suggests a reasonably good representation. Moreover, in the SSESA region, the interquartile range was reduced relative to the CMIP3 analysis, which indicates a lower dispersion between the CMIP5 *versus* the CMIP3 models. The opposite situation was found for the SEBR region with higher dispersion among CMIP5 than CMIP3 simulations.

5. Summary and conclusions

The nature of the projected changes in precipitation showing areas of increase in the tropics and high latitudes and decrease in the subtropics (Knutti and Sedláček, 2013) suggests a need for a model evaluation at the regional scale. The aim of this study was to assess the ability of two sets of GCMs to represent summer, winter, and annual precipitation in South America, south of the equator, and in three sub-regions (CSA, SEBR, and SSESA) between years 1960 and 1999. Monthly precipitation simulations corresponding to the 20th century derived from 19 GCMs from CMIP3 multi-model data set and an equal number of GCMs from CMIP5 data set were analysed. A subset of eight GCMs from each intercomparison projects was considered for the comparative analysis between the two generations of climate models.

The areas where GCMs represent adequate precipitation, as well as the ones where they under- or overestimate it, were identified by calculating the relative bias as the percentage of observed precipitation which is simulated by each GCMs' ensemble. Results from this analysis indicate that summer precipitation is adequately represented by both CMIP3 and CMIP5 models' ensembles particularly in CSA and in parts of the SSESA and SEBR regions. However, both ensembles display some differences. In DJF, the relative bias over Amazonia, central South America, eastern Argentina, and Uruguay is reduced in CMIP5 compared with CMIP3. In JJA, the same occurs in some areas of Amazonia. Annual precipitation was also better represented by the CMIP5 GCMs as they underestimate precipitation to a lesser extent than CMIP3, although CMIP5 overestimation values in NE Brazil were much larger than those in the CMIP3 analysis.

The individual GCM performance was evaluated by a spatial correlation analysis between the seasonal and annual precipitation patterns from the observed gridded data set and those derived from the simulations. As there was not a single optimal model that accurately represented the South American summer, winter, and annual rainfall,

Table 3. CMIP3 GCMs with the highest linear spatial correlation coefficients between the observed and simulated precipitation for different regions and seasons.

Season	Region			
	South America	CSA	SEBR	SSESA
DJF	Ensemble 19 ($R=0.73$)	Ensemble 19 ($R=0.92$)	Ensemble 19 ($R=0.92$)	Ensemble 19 ($R=0.88$)
	Ensemble 8 ($R=0.75$)	Ensemble 8 ($R=0.96$)	Ensemble 8 ($R=0.91$)	Ensemble 8 ($R=0.89$)
	MRI-CGCM2.3.2 ($R=0.79$)	MIROC3.2(hires) ($R=0.94$)	MIROC3.2(hires) ($R=0.94$)	MIROC3.28(hires) ($R=0.93$)
JJA	Ensemble 19 ($R=0.63$)	Ensemble 19 ($R=0.67$)	Ensemble 19 ($R=0.75$)	Ensemble 19 ($R=0.87$)
	Ensemble 8 ($R=0.74$)	Ensemble 8 ($R=0.76$)	Ensemble 8 ($R=0.81$)	Ensemble 8 ($R=0.89$)
	UKMO-HadGEM1 ($R=0.80$)	GFDL-CM2.0 ($R=0.85$)	MRI-CGCM2.3.2 ($R=0.83$)	MRI-CGCM2.3.2 ($R=0.95$)
Annual	Ensemble 19 ($R=0.64$)	Ensemble 19 ($R=0.96$)	Ensemble 19 ($R=0.83$)	Ensemble 19 ($R=0.70$)
	Ensemble 8 ($R=0.67$)	Ensemble 8 ($R=0.95$)	Ensemble 8 ($R=0.63$)	Ensemble 8 ($R=0.75$)
	MRI-CGCM2.3.2 ($R=0.80$)	MRI-CGCM2.3.2 ($R=0.93$)	MIROC3.2(hires) ($R=0.84$)	MIROC3.2(hires) ($R=0.80$)

The correlations with the 19 and 8 multi-model ensembles are also indicated.

Table 4. CMIP5 GCMs with the highest linear spatial correlation coefficients between the observed and simulated precipitation for different regions and seasons.

Season	Region			
	South America	CSA	SEBR	SSESA
DJF	Ensemble 19 ($R=0.73$)	Ensemble 19 ($R=0.96$)	Ensemble 19 ($R=0.93$)	Ensemble 19 ($R=0.87$)
	Ensemble 8 ($R=0.72$)	Ensemble 8 ($R=0.96$)	Ensemble 8 ($R=0.91$)	Ensemble 8 ($R=0.88$)
	HadCM3 HadGEM2-ES ($R=0.77$)	MRI-CGCM3 ($R=0.88$)	MIROC4h ($R=0.93$)	MIROC4h ($R=0.92$)
JJA	Ensemble 19 ($R=0.71$)	Ensemble 19 ($R=0.77$)	Ensemble 19 ($R=0.83$)	Ensemble 19 ($R=0.94$)
	Ensemble 8 ($R=0.73$)	Ensemble 8 ($R=0.74$)	Ensemble 8 ($R=0.86$)	Ensemble 8 ($R=0.95$)
	HadGEM2-CC ($R=0.84$)	MIROC4h ($R=0.90$)	MRI-CGCM3 ($R=0.95$)	MRI-CGCM3 ($R=0.93$)
Annual	Ensemble 19 ($R=0.67$)	Ensemble 19 ($R=0.96$)	Ensemble 19 ($R=0.90$)	Ensemble 19 ($R=0.76$)
	Ensemble 8 ($R=0.66$)	Ensemble 8 ($R=0.94$)	Ensemble 8 ($R=0.86$)	Ensemble 8 ($R=0.79$)
	HadGEM2-ES ($R=0.79$)	INMCM4 ($R=0.94$)	MIROC4h ($R=0.86$)	NorESM1-M ($R=0.87$)

The correlations with the 19 and 8 multi-model ensembles are also indicated.

the best models in each season and region are summarized in Tables 3 (CMIP3) and 4 (CMIP5). These tables also include the results for the multi-model ensembles for the 19 GCMs considered from each intercomparison project. In order to make a fair comparison to evaluate whether there have been any improvement in the regional representation of rainfall in CMIP5, results for the subset of eight GCMs that belong to the same institutions are also included (Tables 1 and 2). MIROC3.2 (hires) showed the best representation of summer precipitation in the three sub-regions considering the CMIP3 models, whereas MIROC4h, from the same institution, was the best in the SEBR and SSESA regions among the CMIP5 simulations. In both cases, these models are among those with highest spatial resolution suggesting that this could be a relevant issue for an adequate estimation of rainfall in the analysed regions. Moreover, most of the precipitation in these regions are associated with heavy rainfall events (Re and Barros, 2009) and extreme precipitation is dependent on resolution (Randall *et al.*, 2007) . In the CSA region, the ensembles of the 19 CMIP5 GCMs, as well as the 8 GCMs' subset, followed by the MRI-CGCM3 model, showed the highest correlation coefficients. During winter, precipitation in the SEBR region was more adequately represented by the MRI-CGCM2.3.2 (CMIP3) and MRI-CGCM3 (CMIP5) models, both belonging to the same institution. The ensembles of the eight CMIP3 models (Table 3) did not stand as those with best representation of rainfall in any of the three sub-regions, with the exception of summer precipitation in the CSA region. For the new generation of GCMs (Table 4), the ensemble of eight CMIP5 models represented more adequately the winter rainfall in SSESA.

Analysis of area averages of GCMs for each of the sub-regions showed that the highest dispersion between models was found in SSESA in all the analysed seasons, indicating the difficulties of most models to represent the processes leading to precipitation in this region. Models represented summer precipitation patterns more adequately than for other seasons. However, though CMIP5 GCMs still underestimated precipitation, they did so to a lesser extent than those of CMIP3, and the dispersion among CMIP5 models was smaller than in the CMIP3 case. The comparative analysis of relative errors for the eight climate models belonging to the same institutions showed that the models' ensembles agree with observations better than the corresponding typical model. Only the MRI-CGCM2.3.2 model of CMIP3 exhibited a better performance than the multi-model ensemble while there was no individual GCM in the CMIP5 set showing the same result.

The median nRMSE of CMIP5 models was higher for summer, winter, and the annual mean than for the CMIP3 models. However, the errors of the ensemble means were lower for CMIP5 models for the winter and annual cases.

The analysis carried out in this study diagnosed the errors in the representation of South American rainfall in two generations of climate models. Our results are in line with previous studies showing that the multi-model ensemble is the most robust tool to represent observed spatial patterns. Only in some regions and seasons, single GCMs [MIROC3.2(hires) – CMIP3 – and MIROC4h – CMIP5] presented better results than the ensemble. Finally, it is important to highlight that although it was possible to identify some improvements in the rainfall representation in particular regions and seasons, the diagnostic analysis presented in this study does not allow attributing them to specific changes between CMIP3 and CMIP5 versions of the evaluated models.

Acknowledgements

This research was supported by the University of Buenos Aires, UBACYT-20020100100803, Consejo Nacional de Investigaciones Científicas y Técnicas, PIP2009-00444, and Agencia Nacional de Promoción Científica y Tecnológica, PICT07-00400. We acknowledge the Climate Research Unit (CRU) for providing the monthly gridded precipitation data and also the Program for Climate Model Diagnosis and Intercomparison (PCMDI) for collecting and archiving the data of CMIP3 and CMIP5 models. The authors wish to thank anonymous referees and Dr Pablo Rabinowicz for their valuable comments and helpful advice.

References

Alves LM, Marengo J. 2010. Assessment of regional seasonal predictability using the PRECIS regional climate modeling system over South America. *Theor. Appl. Climatol.* **100**: 337–350, DOI: 10.1007/s00704-009-0165-2.

Barros VR. 2006. Tendencias climáticas e hidrológicas en la cuenca del Plata. In *El cambio climático en la Cuenca del Plata*, Barros V, Clarke R, Silva Dias P (eds). CIMA: Buenos Aires, Argentina; 12–18 (in Spanish).

Bellouin N, Boucher O, Haywood J, Johnson C, Jones A, Rae J, Woodward S. 2007. Improved representation of aerosols for HadGEM2. Hadley Centre Technical Note 73. Met Office Hadley Centre: Exeter, UK.

Berbery EH, Doyle M, Barros V. 2006. Tendencias regionales en la precipitación. In *El cambio climático en la Cuenca del Plata*, Barros V, Clarke R, Silva Dias P (eds). CIMA: Buenos Aires, Argentina; 67–79 (in Spanish).

Boulanger J-P, Martinez F, Segura EC. 2007. Projection of future climate change conditions using IPCC simulations, neural networks and Bayesian statistics. Part 2: precipitation mean state and seasonal cycle in South America. *Clim. Dyn.* **28**: 255–271, DOI: 10.1007/s00382-006-0182-0.

Delworth TL, Broccoli AJ, Rosati A, Stouffer RJ, Balaji V, Beesley JA, Cooke WF, Dixon KW, Dunne J, Dunne KA, Durachta JW, Findell KL, Ginoux P, Gnanadesikan A, Gordon CT, Griffies SM, Gudgel R, Harrison MJ, Held IM, Hemler RS, Horowitz LW, Klein SA, Knutson TR, Kushner PJ, Langenhorst AR, Lee H-C, Lin S-J, Lu AJ, Malyshev SL, Milly PCD, Ramaswamy FV, Russell J, Schwarzkopf MD, Shevliakova E, Sirutis JJ, Spelman MJ, Stern WF, Winton M, Wittenberg AT, Wyman B, Zeng F, Zhang R. 2006. GFDL's CM2 global coupled climate models. Part I: formulation and simulation characteristics. *J. Clim.* **19**(5), DOI: 10.1175/JCLI3629.1.

Doyle M, Barros V. 2011. Attribution of the river flow growth in the Plata Basin. *Int. J. Climatol.* **31**: 2234–2248, DOI: 10.1002/joc.2228.

Dufresne J-L, Foujols M-A, Denvil S, Caubel A, Marti O, Aumont O, Balkanski Y, Bekki S, Bellenger H, Benshila R, Bony S, Bopp L, Braconnot P, Brockmann P, Cadule P, Cheruy F, Codron F, Cozic A, Cugnet D, de Noblet N, Duvel J-P, Ethé C, Fairhead L, Fichefet T, Flavoni S, Friedlingstein P, Grandpeix J-Y, Guez L, Guilyardi E, Hauglustaine D, Hourdin F, Idelkadi A, Ghattas J, Joussaume S, Kageyama M, Krinner G, Labetoulle S, Lahellec A, Lefebvre M-P, Lefevre F, Levy C, Li ZX, Lloyd J, Lott F, Madec G, Mancip M, Marchand M, Masson S, Meurdesoif Y, Mignot J, Musat I, Parouty S, Polcher J, Rio C, Schulz M, Swingedouw D, Szopa S, Talandier C, Terray P, Viovy N, Vuichard N. 2013. Climate change projections using the IPSL-CM5 Earth System Model: from CMIP3 to CMIP5. *Clim. Dyn.* **40**(9–10): 2123–2165.

Flato G, Marotzke J, Abiodun B, Braconnot P, Chou SC, Collins W, Cox P, Driouech F, Emori S, Eyring V, Forest C, Gleckler P, Guilyardi E, Jakob C, Kattsov V, Reason C, Rummukainen M. 2013. Evaluation of climate models. In *Climate Change 2013. The Physical Science Basis. Contribution of Working Group I to the Fifth Assessment Report of the Intergovernmental Panel on Climate Change*, Stocker TF, Qin D, Plattner G-K, Tignor M, Allen SK, Boschung J, Nauels A, Xia Y, Bex V, Midgley PM (eds). Cambridge University Press: Cambridge, UK and New York, NY; 741–866.

Gan M, Rao VB, Moscati CL. 2006. South American monsoon indices. *Atmos. Sci. Lett.* **6**: 2219–2223, DOI: 10.1002/ASL.119.

Giorgi F. 2002. Variability and trends of sub-continental scale surface climate in the twentieth century. Part I: observations. *Clim. Dyn.* **18**: 675–691, DOI: 10.1007/s00382-001-0204-x.

Gleckler PJ, Taylor KE, Doutriaux C. 2008. Performance metrics for climate models. *J. Geophys. Res.* **113**: D06104, DOI: 10.1029/2007JD008972.

Gulizia C, Camilloni I, Doyle M. 2013. Identification of the principal patterns of summer moisture transport in South America and their representation by WCRP/CMIP3 global climate models. *Theor. Appl. Climatol.* **112**: 227–241, DOI: 10.1007/s00704-012-0729-4.

Harris I, Jones PD, Osborn TJ, Lister DH. 2013. Updated high-resolution grids of monthly climatic observations. *Int. J. Climatol.* **34**: 623–642, DOI: 10.1002/joc.3711.

Haylock MR, Peterson TC, Alves LM, Ambrizzi T, Anunciação YMT, Baez J, Barros VR, Berlato MA, Bidegain M, Coronel G, Corradi V, Garcia VJ, Grimm AM, Karoly D, Marengo JA, Marino MB, Moncunill DF, Nechet D, Quintana J, Rebello E, Rusticucci M, Santos JL, Trebejo I, Vincent LA. 2006. Trends in total and extreme South American rainfall in 1960–2000 and links with sea surface temperature. *J. Clim.* **19**: 1490–1512, DOI: 10.1175/JCLI3695.1.

Insel N, Poulsen C, Ehlers T. 2010. Influence of the Andes Mountains on South American moisture transport, convection, and precipitation. *Clim. Dyn.* **35**: 1477–1492, DOI: 10.1007/s00382-009-0637-1.

IPCC. 2007. *Climate Change. The Scientific Basis*. Cambridge University Press: Geneva, Switzerland.

Joetzjer E, Douville H, Delire C, Ciais P. 2013. Present-day and future Amazonian precipitation in global climate models: CMIP5 versus CMIP3. *Clim. Dyn.* **41**(11–12): 2921–2936, DOI: 10.1007/s00382-012-1644-1.

Jones C, Carvalho L. 2013. Climate change in the South American monsoon system: present climate and CMIP5 projections. *J. Clim.* **26**: 6660–6678, DOI: 10.1175/JCLI-D-12-00412.1.

Knutti R, Sedláček J. 2013. Robustness and uncertainties in the new CMIP5 climate model projections. *Nat. Clim. Change* **3**: 369–373, DOI: 10.1038/nclimate1716.

Lenters JD, Cook KH. 1995. Simulation and diagnosis of the regional summertime precipitation climatology of South America. *J. Clim.* **8**: 2298–3005,DOI: 10.1175/1520-0442(1995)008<2988:SADOTR>2.0.CO;2.

Marengo JA, Rusticucci M, Penalba O, Renom M. 2010. An intercomparison of observed and simulated extreme rainfall and temperature events during the last half of the twentieth century: part 2: historical trends. *Clim. Change* **98**: 509–529, DOI: 10.1007/s10584-009-9743-7.

Meehl GA, Covey C, Delworth TL, Latif M, McAveney B, Mitchell JFB, Stouffer RJ, Taylor KE. 2007. The WCRP CMIP3 multimodel dataset: a new era in climate change research. *Bull. Am. Meteorol. Soc.* **88**: 1383–1394, DOI: 10.1175/BAMS-88-9-1383.

Pincus R, Batstone CP, Hofmann RJP, Taylor KE, Gleckler PJ. 2008. Evaluating the present-day simulation of clouds, precipitation, and radiation in climate models. *J. Geophys. Res.* **113**: D14209, DOI: 10.1029/2007JD009334.

Popescu I, Brandimarte L, Perera MSU, Peviani M. 2012. Assessing residual hydropower potential of the La Plata Basin accounting for future user demands. *Hydrol. Earth Syst. Sci.* **16**: 2813–2823.

Prohaska F. 1976. The climate of Argentina, Paraguay and Uruguay. In *Climates of Central and South America. World Survey of Climatology*, Vol. **12**, Schwerdtfeger W (ed). Elsevier: Amsterdam; 13–72.

Randall DA, Wood RA, Bony S, Colman R, Fichefet T, Fyfe J, Kattsov V, Pitman A, Shukla J, Srinivasan J, Stouffer RJ, Sumiand A, Taylor KE. 2007. Cilmate models and their evaluation. In *Climate Change 2007: The Physical Science Basis. Contribution of Working Group I to the Fourth Assessment Report of the Intergovernmental Panel on Climate Change*, Solomon S, Qin D, Manning M, Chen Z, Marquis M, Averyt KB, Tignor M, Miller HL (eds). Cambridge University Press: Cambridge, UK and New York, NY.

Re M, Barros V. 2009. Extreme rainfalls in SE South America. *Clim. Change* **96**: 119–136.

Rusticucci M, Barrucand M. 2004. Observed trends and changes in temperature extremes over Argentina. *J. Clim.* **17**: 4099–4107, DOI: 10.1175/1520-0442(2004)017<4099:OTACIT>2.0.CO;2.

Sakaguchi K, Zeng X, Brunke MA. 2012. Temporal- and spatial-scale dependence of three CMIP3 climate models in simulating the surface temperature trend in the twentieth century. *J. Clim.* **25**: 2456–2470, DOI: 10.1175/JCLI-D-11-00106.1.

Schaller N, Mahlstein I, Cermak J, Knutti R. 2011. Analyzing precipitation projections: a comparison of different approaches to climate model evaluation. *J. Geophys. Res.* **116**: D10118, DOI: 10.1029/2010JD014963.

Seth A, Rojas M, Rauscher S. 2010. CMIP3 projected changes in the annual cycle of the South American Monsoon. *Clim. Change* **98**: 331–357, DOI: 10.1007/s10584-009-9736-6.

Silvestri G, Vera C. 2008. Evaluation of the WCRP-CMIP3 model simulations in the La Plata Basin. *Meteorol. Appl.* **15**: 497–502, DOI: 10.1002/met.98.

Stouffer RJ, Taylor KE, Meehl GA. 2011. CMIP5 long-term experimental design. *CLIVAR Exch.* **56**: 5–7.

Su F, Duan X, Chen D, Hao Z, Cuo L. 2013. Evaluation of the global climate models in the CMIP5 over the Tibetan Plateau. *J. Clim.* **26**: 3187–3208.

Taylor KE, Stouffer RJ, Meehl GA. 2012. An Overview of CMIP5 and the experiment design. *Bull. Am. Meteorol. Soc.* **93**: 485–498, DOI: 10.1175/BAMS-D-11-00094.1.

Watanabe S, Hajima T, Sudo K, Nagashima T, Takemura T, Okajima H, Nozawa T, Kawase H, Abe M, Yokohata T, Ise T, Sato H, Kato E, Takata K, Emori S, Kawamiya M. 2011. MIROC-ESM: model description and basic results of CMIP5-20c3m experiments. *Geosci. Model Dev. Discuss.* **4**: 1063–1128.

Wilcox LJ, Charlton-Perez AJ, Gray LJ. 2012. Trends in Austral jet position in ensembles of high- and low-top CMIP5 models. *J. Geophys. Res.* **117**: D13115, DOI: 10.1029/2012JD017597.

Wilks D. 1995. *Statistical Methods in the Atmospheric Sciences*. Academic Press: San Diego, CA; 24–25.

Willmott C, Matsuura K. 2005. Advantages of the mean absolute error (MAE) over the root mean square error (RMSE) in assessing average model performance. *Clim. Res.* **30**: 79–82.

Yin L, Fu R, Shevliakova E, Dickinson R. 2012. How well can CMIP5 simulate precipitation and its controlling processes over tropical South America? *Clim. Dyn.* **41**(11–12): 3127–3143, DOI: 10.1007/s00382-012-1582-y.

